Technical Document 2278
April 1992

Using the Burst Derivative Measure to Improve the Computational Efficiency of ISAR Motion Compensation Algorithms

R. P. Bocker
S. A. Jones

Technical Document 2278
April 1992

Using the Burst Derivative Measure to Improve the Computational Efficiency of ISAR Motion Compensation Algorithms

R. P. Bocker
S. A. Jones

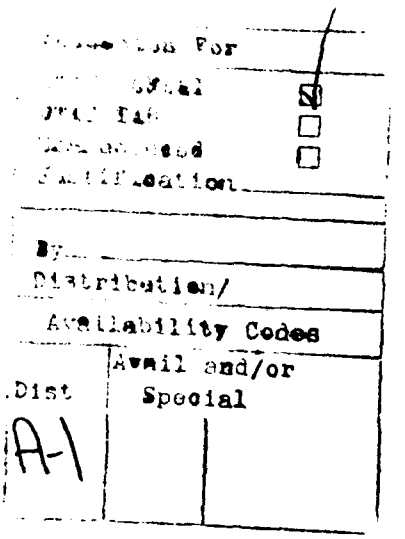

NAVAL COMMAND, CONTROL AND OCEAN SURVEILLANCE CENTER
RDT&E DIVISION
San Diego, California 92152-5000

J. D. FONTANA, CAPT, USN
Commanding Officer

R. T. SHEARER
Executive Director

ADMINISTRATIVE INFORMATION

The work documented in this report was performed by Richard P. Bocker of the Processing Research and Development Branch (Code 761) and Scott A. Jones of the Radar Branch (Code 755), Naval Command, Control and Ocean Surveillance Center RDT&E Division.

Released by
G. W. Byram, Head
Processing Research and
Development Branch

Under authority of
J. R. Wangler, Head
Space Systems and Technology
Division

ACKNOWLEDGMENTS

Work on the translational motion compensation (TMC) algorithm was supported by the Strategic Defense Initiative Organization, Innovative Science and Technology Office, (SDIO/TI) through the Office of Naval Research (Document No. N00014-91-WX2C021) managed by Dr. Keith Bromley. Work on the rotational motion compensation (RMC) algorithm was supported by the Office of Naval Research (Document No. N00014-92-WX22222) managed by Mr. William Miceli.

SUMMARY

Inverse synthetic aperture radar (ISAR) is an imaging technique that shows great promise in classifying airborne targets in realtime under all weather conditions. Over the past several years, a large body of ISAR data has been collected and considerable effort has been expended to develop algorithms to form high-resolution images from these data. One important goal of workers in this field is to develop software that will do the best job of imaging under the widest range of conditions. The success of classifying targets using ISAR is predicated upon forming highly focused radar images of these targets. Efforts to develop highly focused imaging computer software have been challenging, mainly because the imaging depends on and is affected by the motion of the target, which in general is not known. Specifically, the target usually has both rotational motion about some axis and translational motion as a whole with respect to the imaging radar. The slant-range translational motion kinematic quantities of the target must be first accurately estimated from the radar data and compensated before a focused image can be formed. Following slant-range translational motion compensation, the image is further focused by determining and correcting for target rotation.

We propose the use of the burst derivative measure as a means to improve the computational efficiency of currently used motion compensation ISAR algorithms. This technical report describes the use of the burst derivative measure in motion compensation ISAR algorithms for estimating both the slant-range translational motion and rotational kinematic quantities of an uncooperative airborne target. Tests have been performed on simulated as well as actual ISAR data using both a Sun 4 SPARCstation 2 and a parallel processing transputer array. Preliminary results indicate that the burst derivative measure gives significant improvement in processing speed over the traditional entropy measure presently employed.

CONTENTS

FIGURES

1.0 INTRODUCTION

Potentially the most powerful means to rapidly classify airborne targets at long range under all weather conditions is through the use of some type of imaging radar (Ausherman et al., 1984). Inverse synthetic aperture radar (ISAR) is one technique that shows real promise in this area (Wehner, 1987). Scientists and engineers at the RDT&E Division of the Naval Command, Control and Ocean Surveillance Center (NCCOSC) in San Diego have developed microwave stepped-frequency ISAR systems as well as the algorithms, software, and processing architectures necessary to process ISAR signal returns for displaying highly focused ISAR images.

The translational motion compensation (TMC) algorithm, one of two computationally intensive ISAR algorithms presently employed, estimates the slant-range translational velocity, acceleration, and jerk of an uncooperative target with respect to the imaging radar. The determination of the target's translational kinematic information is the first important step toward achieving a highly focused ISAR image. The input to the TMC algorithm is a two-dimensional unprocessed ISAR spatial frequency spectrum. This spectrum is multiplied by a spatial frequency filter containing initial guess information of the target's slant-range translational velocity, acceleration, and jerk. The resulting filtered spectrum is then Fourier transformed using the two-dimensional fast Fourier transform (2D-FFT) algorithm. The sharpness of the resulting space domain ISAR image is determined by computing its entropy. This process is repeated a number of times using different values of velocity, acceleration, and jerk in the spatial frequency filter. Those values that give rise to an ISAR image having minimum entropy are used as the best estimates of the target's actual slant-range translational velocity, acceleration, and jerk. Once the translational kinematic estimates have been determined, then processing may advance to the second stage where the rotational kinematics of the target are estimated using the rotational motion compensation (RMC) algorithm. The RMC algorithm is used to further improve the sharpness of the translational motion-compensated ISAR image obtained as the output of the TMC algorithm.

The authors have been investigating the use of a new measure, which we call the burst derivative measure, as an alternative means for estimating the slant-range translational and rotational kinematic quantities of an airborne target. The burst derivative measure is an outgrowth of an earlier NCCOSC RDT&E Division attempt in using the Fisher measure (Frieden, 1989, 1990) as a means to improve the computational throughput rates of the TMC and RMC algorithms.

The burst derivative measure offers a significant speed advantage over the entropy measure in that computations may be confined strictly to the spatial frequency domain. Hence, the numerous 2D-FFTs presently required using the entropy measure in the TMC and the RMC algorithms could be avoided. This technical report describes preliminary results on the use of the burst derivative measure in estimating the translational and rotational kinematics of an uncooperative airborne target.

In the following sections, we will present the underlying theory pertinent to the formation of the motion-compensated ISAR image. We first begin our discussion with a description of the ISAR geometry, the formation of the unprocessed ISAR spatial frequency spectrum, a description of the TMC and RMC algorithms, and finally preliminary results for both simulated as well as real aircraft data.

2.0 ISAR GEOMETRY

The geometry employed for the ISAR scenario is depicted in figure 1. For pedagogical purposes, lets consider a two-dimensional aircraft moving in a plane. A stationary ground-based radar (assumed to be a monostatic omnidirectional transmitter and receiver for simplicity) is located at the origin of a right-handed Cartesian coordinate system XY. A solid extended aircraft is moving relative to the ground-based radar. The center of mass of this aircraft is located at the origin of a second right-handed Cartesian coordinate system xy whose corresponding axes are parallel to those of XY. In addition, a third right-handed Cartesian coordinate system $x'y'$, attached to the aircraft, is used in describing the rotation of the aircraft with respect to the xy system. The origins of xy and $x'y'$ are coincident. The angular displacement, $\theta(t)$, describes the rotational position of the aircraft relative to xy. The slant-range, $r(t)$, describes the translational position of the aircraft's center of mass relative to the radar. Recall from classical mechanics that the overall motion of an extended rigid body can be described by the translational motion of its center of mass plus the rotational motion of the object about its center of mass. The slant-range, $r(t)$, is of paramount importance in the translational motion description, whereas angular displacement, $\theta(t)$, is vitally important in the rotational motion description.

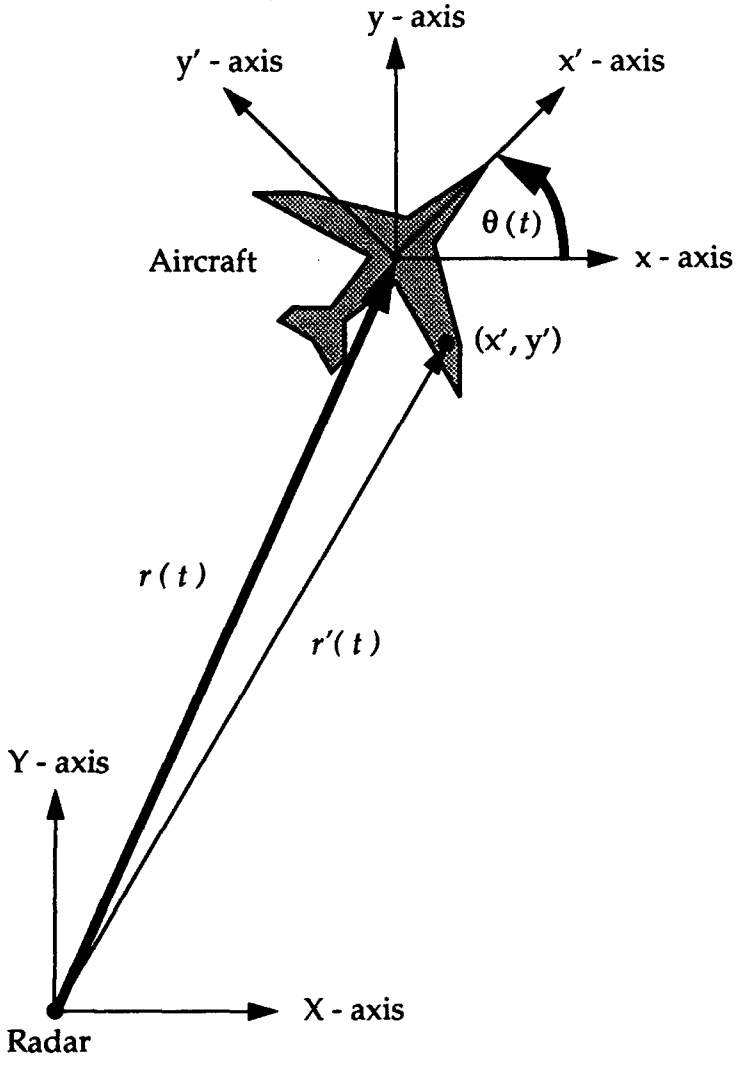

Figure 1. Inverse synthetic aperture radar geometry.

3.0 FORMATION OF THE UNPROCESSED ISAR SPATIAL FREQUENCY SPECTRUM

Presented in this section is the underlying theory describing the formation of the unprocessed ISAR spatial frequency spectrum. This spectrum results from the detection of the radar return from the moving aircraft illuminated by a linear stepped-frequency modulated radar signal.

The moving aircraft is actively illuminated by the ground-based radar transmitter. The transmitted radar signal is a stepped-frequency modulated waveform as depicted in figure 2. The quantities f and t represent temporal frequency and time, respectively. This waveform consists of N bursts; each burst contains M pulses. Each transmitted pulse may be thought of as a quasi-monochromatic spherical wave that briefly illuminates the entire aircraft. This gives rise to a coherent reflected (scattered) return. The return pulse is quadrature-detected at the radar receiver and heterodyned to yield a single complex number. The MN complex numbers obtained from the entire transmitted radar signal may be organized into a two-dimensional (M by N matrix) array of numbers. This array represents the unprocessed ISAR spatial frequency spectrum of the aircraft. To understand how this spatial frequency spectrum is generated from a quantitative point of view, we will next show analytically how a single complex spatial frequency spectral value arises from a single radar pulse.

3.1 SINGLE-PULSE ILLUMINATION

A single transmitted radar pulse may be represented by a quasi-monochromatic spherically expanding wave. The analytic wave function representation of this pulse is given by

$$\psi_T(r', t) = A \frac{exp[-i2\pi ft] exp[i2\pi (f/c) r']}{r'}, \quad (1)$$

where A is the amplitude, f the temporal frequency, t the time, r' the distance from

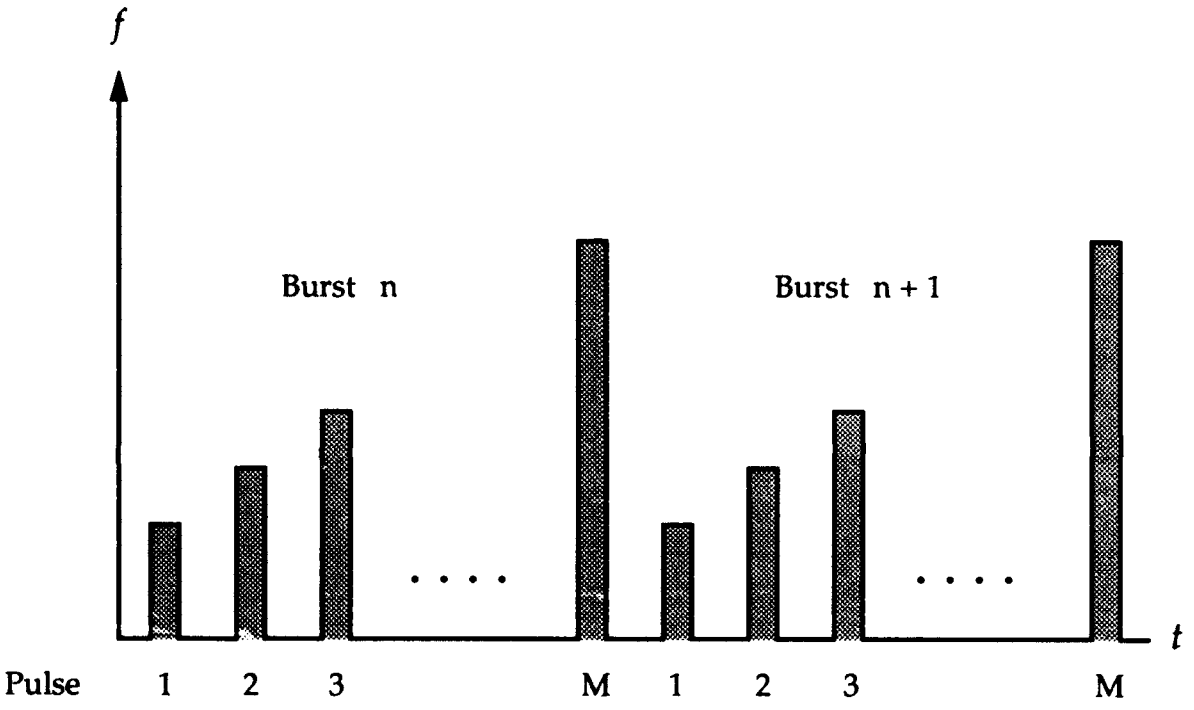

Figure 2. Stepped-frequency modulated transmitted radar signal.

the center of the expanding spherical wave (see figure 1) to a point in space, and c the speed of light in vacuum. The aircraft is made up of a distribution of point scatterers. Figure 1 depicts the position of one such point scatterer located at the coordinates (x', y'). The infinitesimal reflected return from this point scatterer, as seen from the radar, is given by

$$d\psi_R(r', t) = A \frac{exp[-i2\pi ft]\, exp[i4\pi (f/c) r']}{(r')^2} \rho(x', y')\, dx'dy'. \quad (2)$$

The function $\rho(x', y')$ represents the reflectivity density of the aircraft and $dx'dy'$ is an infinitesimal differential area element centered about the point (x', y'). With the use of the principle of superposition, the radar return for a single pulse due to the entire aircraft is obtained by integrating equation 2. We obtain

$$\psi_R(t) = exp[-i2\pi ft] \int_{-\infty}^{\infty}\int_{-\infty}^{\infty} h(x', y')\ exp[i4\pi (f/c) r']\ dx'dy', \quad (3)$$

where by definition

$$h(x', y') \equiv \frac{A}{(r')^2} \rho(x', y'). \quad (4)$$

It is worth mentioning at this point that the formation of the final focused ISAR image is equivalent to estimating the reflectivity density function $\rho(x', y')$ or equivalently $h(x', y')$. The radar pulse return is detected and heterodyned at the radar receiver, yielding a single complex spatial frequency spectral value

$$U = \int_{-\infty}^{\infty}\int_{-\infty}^{\infty} h(x', y')\ exp[i4\pi (f/c) r']\ dx'dy'. \quad (5)$$

For this analysis, we will assume that the aircraft is located in the far field of the radar and that the dimensions of the aircraft are small in comparison to the distance $r(t)$. Using the far-field approximation (Goodman, 1968), we may approximate the quantity r'

appearing in the exponent of equation 5 by the expression

$$r' \approx r + x' \sin\theta + y' \cos\theta. \tag{6}$$

The quantity r' appearing in the denominator of equation 4 may be approximated by r when using the far-field approximation. Equation 5 can be rewritten as

$$U = exp[i4\pi (f/c) r] \quad H, \tag{7}$$

where by definition

$$H \equiv \int_{-\infty}^{\infty} \int_{-\infty}^{\infty} h(x', y') \quad exp[i2\pi (px' + qy')] \quad dx'dy' \tag{8}$$

and

$$p \equiv 2 (f/c) \sin\theta \qquad \text{and} \qquad q \equiv 2 (f/c) \cos\theta. \tag{9}$$

It is important to note that the quantity U appearing in equation 7 represents a single spatial frequency spectral value only. In this analysis, the aircraft may be regarded as being stationary during the time interval in which the aircraft is illuminated by the single pulse. Hence, the quantities $r(t)$ and $\theta(t)$ are effectively constant in value over this time interval.

3.2 STEPPED-FREQUENCY RADAR ILLUMINATION

The preceding results will now be used to derive a mathematical expression for the two-dimensional spatial frequency spectrum generated by a stepped-frequency radar signal. Keep in mind that between radar pulses the aircraft has moved to a new position, hence $r(t)$ and $\theta(t)$ take on new values for each pulse. During the time interval required to generate one complete frame (M by N array) of spatial frequency spectral data, the slant-range, $r(t)$, and the angular displacement, $\theta(t)$, may be approximated by the first few terms of their MacLaurin series expansions. In particular,

$$r(t) \approx r_o + v_o t + (1/2) a_o t^2 + (1/6) j_o t^3 \tag{10a}$$

$$\theta(t) \approx \theta_o + \omega_o t + (1/2) \alpha_o t^2. \tag{10b}$$

The time $t = 0$ represents the beginning of the frame. The translational kinematic quantities $r_o, v_o, a_o,$ and j_o represent the initial values of the slant-range, velocity, acceleration, and jerk respectively, of the center of mass of the aircraft at time $t = 0$. Likewise, the rotational kinematic quantities $\theta_o, \omega_o,$ and α_o represent the initial values of the angular displacement, velocity, and acceleration, respectively, of the aircraft about its center of mass at $t = 0$. Let the quantity t_{mn} represent the time the aircraft is illuminated by the *mth* pulse of the *nth* burst [henceforth denoted *(m,n)th* pulse], where

$$t_{mn} = [(m-1) + (n-1)M]\,\Delta t. \tag{11}$$

The indices m and n take on the integer values $m = 1, 2, 3, \ldots, M$ and $n = 1, 2, 3, \ldots, N$. The constant Δt represents the time interval between adjacent pulses. Substitution of equation 11 into equations 10a and 10b gives the following expressions for the translational and rotational displacements of the aircraft at the time it is illuminated by the *(m,n)th* pulse

$$r_{mn} \approx r_o + v_o t_{mn} + \frac{1}{2} a_o t_{mn}^2 + \frac{1}{6} j_o t_{mn}^3 \tag{12a}$$

$$\theta_{mn} \approx \theta_o + \omega_o t_{mn} + \frac{1}{2} \alpha_o t_{mn}^2. \tag{12b}$$

With the use of equation 7, the *(m,n)th* pulse gives rise to a single complex spatial frequency spectral value given by

$$U(m,n) = exp[i4\pi (f_m/c) r_{mn}]\; H(m,n), \tag{13}$$

where with the use of equations 8 and 9

$$H(m,n) \equiv \int_{-\infty}^{\infty}\int_{-\infty}^{\infty} h(x',y')\; exp[i2\pi (p_{mn}x' + q_{mn}y')]\; dx'dy' \tag{14}$$

and

$$p_{mn} \equiv 2\,(f_m/c)\,\sin\theta_{mn} \qquad \text{and} \qquad q_{mn} \equiv 2\,(f_m/c)\,\cos\theta_{mn}. \tag{15}$$

The frequency of the *(m,n)th* pulse is given by

$$f_m = f_o + (m-1)\,\Delta f. \tag{16}$$

The quantities f_o and Δf represent the base and step frequencies of the linear stepped-frequency transmitting radar. Hereafter, $H(m, n)$ will be referred to as the ideal translational motion-compensated ISAR spatial frequency spectrum and $U(m, n)$ will be referred to as the unprocessed ISAR spatial frequency spectrum.

4.0 TRANSLATIONAL MOTION COMPENSATION (TMC) ALGORITHM

Presented in this section is a description of the translational motion compensation (TMC) algorithm. The objective of the TMC algorithm is to form an estimate, $\hat{H}(m, n)$, of the ideal translational motion-compensated ISAR spatial frequency spectrum, *H(m, n)*, from the unprocessed ISAR spatial frequency spectrum, $U(m, n)$. To do so requires estimating the translational kinematic quantities v_o, a_o, and j_o.

Equation 13 represents the desired mathematical expression for the *(m,n)th* element of the unprocessed ISAR spatial frequency spectrum. This observable spectrum, in any real application, serves as the input data to the ISAR processing system. Substitution of equation 12a into equation 13 gives

$$U(m, n) = exp\left[i4\pi\,(f_m/c)\,\left(r_o + v_o t_{mn} + \frac{1}{2}a_o t_{mn}^2 + \frac{1}{6}j_o t_{mn}^3\right)\right] H(m, n). \tag{17}$$

At this point, lets indicate which quantities in equation 17 are known and which quantities are to be determined. The spectral values $U(m, n)$ are the known observable inputs to the ISAR processor. The stepped-frequency radar characteristics are known, hence f_m and t_{mn} are also known. The uncooperative aircraft's translational kinematic quantities r_o, v_o, a_o, and j_o are unknown. If these quantities were known,

then it would be a straightforward procedure to solve equation 17 for the ideal spectral values $H(m,n)$. The objective of the TMC algorithm is to estimate the kinematic quantities $v_o, a_o,$ and j_o, which in turn allows us to form estimates of the spatial frequency spectral values, denoted by $\hat{H}(m,n)$. The quantities $\hat{H}(m,n)$ would then serve as the inputs to the RMC algorithm. Again, the RMC algorithm is used to further improve the image sharpness, yielding a highly focused final image $\hat{i}(x,y)$. These ideas are depicted in the flow diagram shown in figure 3.

As previously indicated, the principal objective of the TMC algorithm is to estimate the three translational kinematic quantities $v_o, a_o,$ and j_o. To estimate $v_o, a_o,$ and j_o we first multiply the unprocessed spectral values $U(m,n)$ by a spatial frequency filter function $S(m,n;\hat{v},\hat{a},\hat{j})$. The quantities $\hat{v},\hat{a},$ and $\hat{j}$ appearing in the filter function are initial guesses of the translational velocity, acceleration, and jerk, respectively. This gives

$$\hat{H}(m,n;\hat{v},\hat{a},\hat{j}) = S(m,n;\hat{v},\hat{a},\hat{j})\,U(m,n), \tag{18}$$

where the spatial frequency filter function is mathematically given by

$$S(m,n;\hat{v},\hat{a},\hat{j}) = exp\left[-i4\pi\,(f_m/c)\,(\hat{v}t_{mn} + \frac{1}{2}\hat{a}t_{mn}^2 + \frac{1}{6}\hat{j}t_{mn}^3)\right]. \tag{19}$$

The next step, currently used in the TMC algorithm, is to compute the two-dimensional discrete Fourier transform (2D-DFT), (Gonzalez and Wintz, 1987), of $\hat{H}(m,n;\hat{v},\hat{a},\hat{j})$. In actual ISAR computer implementations, the two-dimensional fast Fourier transform (2D-FFT) algorithm is employed. This gives

$$\hat{h}(x,y;\hat{v},\hat{a},\hat{j}) = \sum_{m=0}^{M-1}\sum_{n=0}^{N-1} \hat{H}(m,n;\hat{v},\hat{a},\hat{j})\,exp\,[i2\pi\,\{x\,(m/M) + y\,(n/N)\}]. \tag{20}$$

The function $\hat{h}(x,y;\hat{v},\hat{a},\hat{j})$ represents an initial estimate of the translational motion-compensated ISAR image. The quality of this image may be determined using entropy as a measure of sharpness. The entropy of the image $\hat{h}(x,y;\hat{v},\hat{a},\hat{j})$ is computed using the equation

$$E(\hat{v},\hat{a},\hat{j}) = \sum_{x=0}^{M-1}\sum_{y=0}^{N-1} \left|\hat{h}(x,y;\hat{v},\hat{a},\hat{j})\right|\;log\left|\hat{h}(x,y;\hat{v},\hat{a},\hat{j})\right|. \tag{21}$$

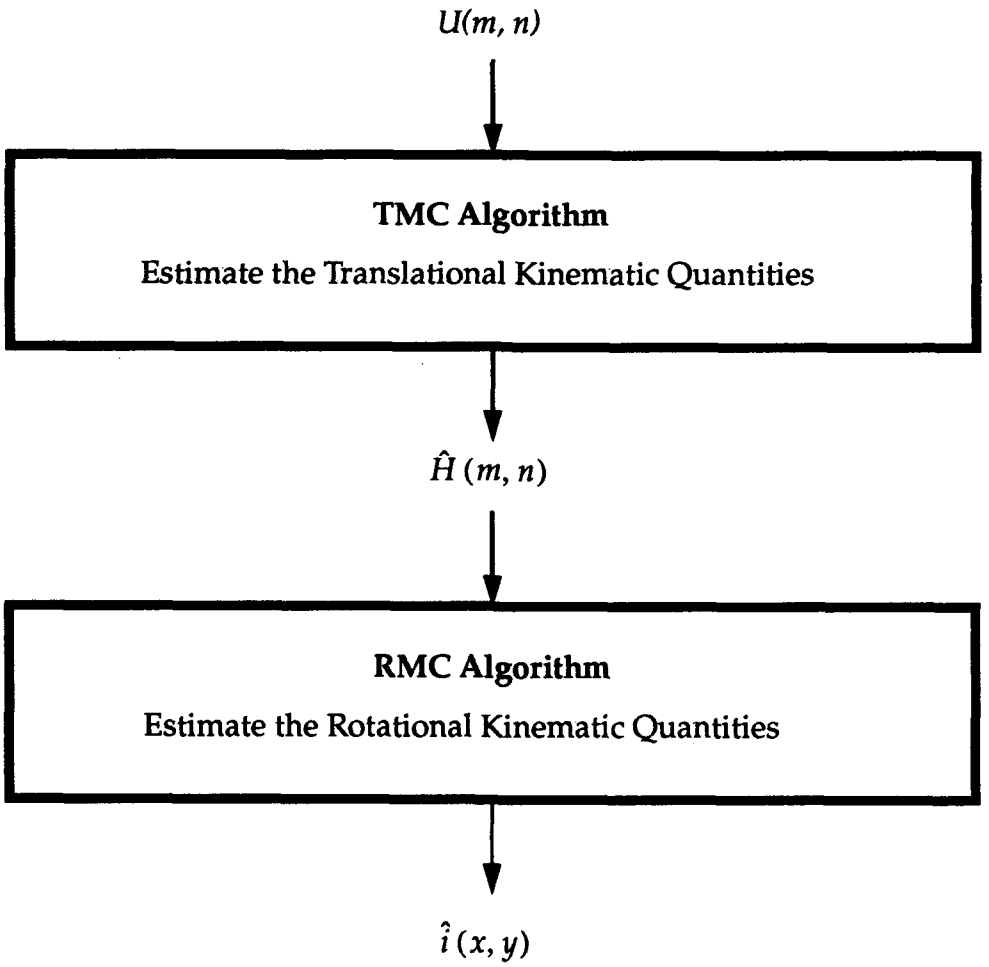

Figure 3. ISAR processing algorithms.

With the help of a search algorithm, this process is iteratively repeated a number of times using different values of $\hat{v}, \hat{a}$, and $\hat{j}$ until a value of velocity, v_e, acceleration, a_e, and jerk, j_e, are obtained that give a minimum value for the entropy.

The values v_e, a_e, and j_e are then used as the best estimates of the target's actual translational velocity, acceleration, and jerk. Once these best estimates have been determined, then the best intermediate translational motion-compensated ISAR image (in terms of sharpness) is the one given by $\hat{h}(x, y)$, where by definition

$$\hat{h}(x, y) \equiv \hat{h}(x, y; v_e, a_e, j_e). \tag{22}$$

Also,

$$\hat{H}(m, n) \equiv \hat{H}(m, n; v_e, a_e, j_e). \tag{23}$$

Note that the phase term in equation 17 containing the quantity r_0 does not affect the overall sharpness of the image $\hat{h}(x, y)$. It does, however, affect the overall positioning (or centering) of the image (in terms of translational shift). Hence, if positioning is of importance, then an estimated value of r_0 can be easily chosen to accomplish a repositioning.

An alternative technique for estimating the velocity, acceleration, and jerk is to use a measure where the computations can be performed strictly in the spatial frequency domain. This would have the advantage of eliminating the numerous 2D-FFTs, which must presently be performed using the entropy measure, in estimating the translational kinematic quantities. The authors have been actively investigating the use of a number of different measures. Based on preliminary simulations, the burst derivative measure shows a great deal of promise as an alternative means for obtaining these translational kinematic estimates. The burst derivative measure is determined by the equation

$$B(\hat{v}, \hat{a}, \hat{j}) = \sum_{m=0}^{M-1} \sum_{n=0}^{N-1} \left| \frac{\partial}{\partial n} \hat{H}(m, n; \hat{v}, \hat{a}, \hat{j}) \right|. \tag{24}$$

As in the case of entropy, the burst derivative measure has been employed successfully with an iterative search algorithm to find estimates of v_e, a_e, and j_e. Once these estimates are obtained, then only one 2D-FFT is required to form the translational motion-compensated ISAR image $\hat{h}(x, y)$ from its estimated translational motion-compensated spectrum $\hat{H}(m, n)$.

5.0 TMC ALGORITHM SIMULATION RESULTS

Preliminary comparisons between the burst derivative measure and the entropy measure in estimating the translational kinematic quantities of an airborne target have been made. These comparisons have been done with simulated as well as actual ISAR data using both a Sun 4 SPARCstation 2 and a parallel processing transputer array. Results typifying the comparison for simulated data on the Sun 4 SPARCstation 2 are presented in this section.

Let's begin by referring to figure 4, which typifies only one of many simulations performed. Figure 4a is a gray-scale plot of the simulated two-dimensional reflectivity density function $\rho(x', y')$ of a fictitious aircraft. The dimensions of this plot correspond to 76 by 76 meters. Each of the point scatterers depicted in this figure have equal reflectivities. For this simulation, the translational kinematic quantities (ground truth) describing the motion of the aircraft at the beginning of the frame were given by

$$r_o = 4400 \ m \qquad v_o = -4.02 \ m/s \qquad a_o = +14.20 \ m/s^2 \qquad j_o = +0.05 \ m/s^3.$$

and the rotational kinematic quantities (ground truth) were given by

$$\theta_o = 90.91 \ deg \qquad \omega_o = -3.25 \ deg/s \qquad \alpha_o = -0.01 \ deg/s^2.$$

The pertinent radar parameters used for this simulation were given by

$$M = 64 \qquad N = 64 \qquad \Delta t = 1.59 \ ms \qquad f_o = 0.372 \ GHz \qquad \Delta f = 2.130 \ MHz.$$

Figure 4b is the gray-scale plot of the unprocessed ISAR spatial frequency spectrum (modulus only plotted). Figure 4c is the gray-scale plot of the unprocessed ISAR image one would obtain by taking the 2D-FFT of the unprocessed ISAR spatial frequency spectrum. If the unprocessed ISAR spatial frequency spectrum is multiplied by the spatial frequency filter given by equation 19 for $\hat{v} = v_o, \hat{a} = 0, \hat{j} = 0$, then the ISAR image that one would obtain from the 2D-FFT operation on the resulting filtered spectrum is shown in figure 4d. Likewise, if the unprocessed ISAR spectrum is multiplied by the spatial frequency filter for $\hat{v} = v_o, \hat{a} = a_o, \hat{j} = 0$, then the ISAR image one would obtain from the 2D-FFT operation on the resulting filtered spectrum is shown in figure 4e. Notice in figure 4e that the aircraft now is readily discernible. Finally,

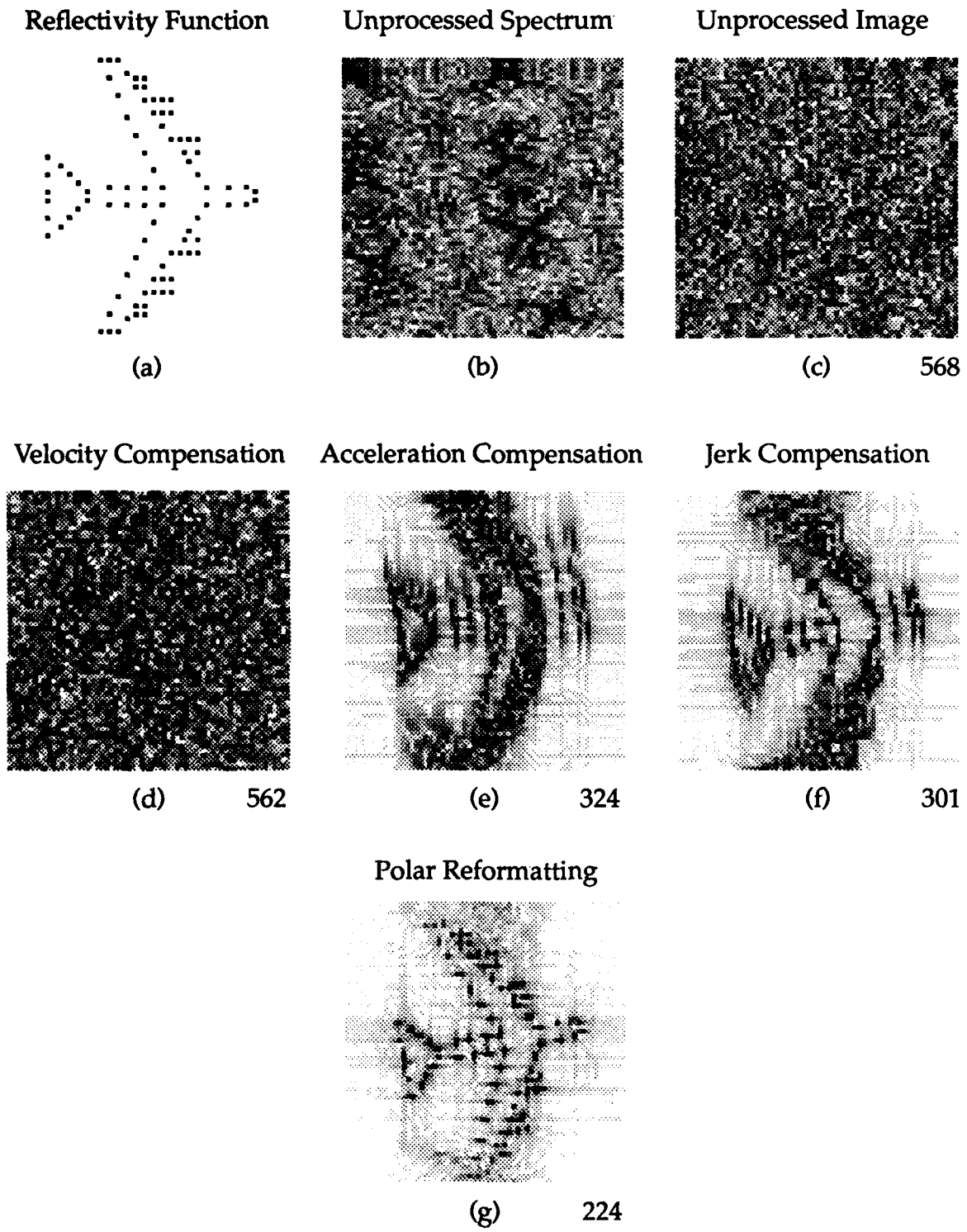

Figure 4. Motion compensation of simulated data using ground truth.

if the unprocessed ISAR spectrum is multiplied by the spatial frequency filter for $\hat{v} = v_o, \hat{a} = a_o, \hat{j} = j_o$, then the ideal translational motion-compensated ISAR image, $h(x,y)$, one would obtain from the 2D-FFT operation on the resulting filtered spectrum is shown in figure 4f. Figure 4f represents about as well as one could hope for in processing the unprocessed ISAR spectrum using a spatial frequency filter containing the actual ground-truth translational kinematics of the moving aircraft.

For comparative purposes, if the translational motion-compensated image obtained in figure 4f is polar-reformatted using the RMC algorithm employing the ground truth rotational kinematic quantities listed on the previous page, then the final ideal rotational motion-compensated (focused) ISAR image, $i(x, y)$, obtained is shown in figure 4g. The results shown in figure 4 will serve as a basis of comparison for similar results obtained using the entropy measure and the burst derivative measure in both the TMC and RMC algorithms for estimating the kinematic quantities. Listed below each subplot in figure 4 are the corresponding entropy values for that subplot. Note, the smaller the value of the entropy, the sharper the image.

Let's now consider the use of the entropy measure in the TMC algorithm for estimating the translational kinematic quantities of the aircraft. Figure 5 shows velocity, acceleration, and jerk slices through the entropy surface described by the entropy function $E(v,a,j)$ defined in equation 21. In particular, figure 5a represents $E(v, 0, 0)$ plotted against v, figure 5b represents $E(v_e, a, 0)$ plotted against a, and figure 5c represents $E(v_e, a_e, j)$ plotted against j. The quantities v_e, a_e, and j_e represent the estimates of the velocity, acceleration, and jerk using the entropy measure. These estimates correspond to the minima of figures 5a, 5b, and 5c, respectively. The triple x symbol in these subplots represents the position of the ground truth values. Those values of velocity, acceleration, and jerk that gave rise to the minimum value of entropy were v_e = -4.1 m/s , a_e = 14.4 m/s^2 , and j_e = 0.00 m/s^3.

Now consider the use of the burst derivative measure in the TMC algorithm for estimating the translational kinematic quantities of the aircraft. Figure 5 also shows velocity, acceleration, and jerk slices through the burst derivative surface described by the burst derivative function $B(v,a,j)$ defined in equation 24. Figure 5d represents $B(v, 0, 0)$ plotted against v, figure 5e represents $B(v_e, a, 0)$ plotted against a, and figure 5f represents $B(v_e, a_e, j)$ plotted against j. The quantities v_e, a_e, and j_e in this case represent the estimates of the velocity, acceleration, and jerk using the burst derivative measure. These estimates correspond to the minima of figures 5d, 5e, and 5f, respectively. Again, the triple x symbol represents the position of the ground truth values. Those values of velocity, acceleration, and jerk that gave rise to the minimum value of burst derivative were v_e = -3.8 m/s , a_e = 14.2 m/s^2 , and j_e = 0.01 m/s^3.

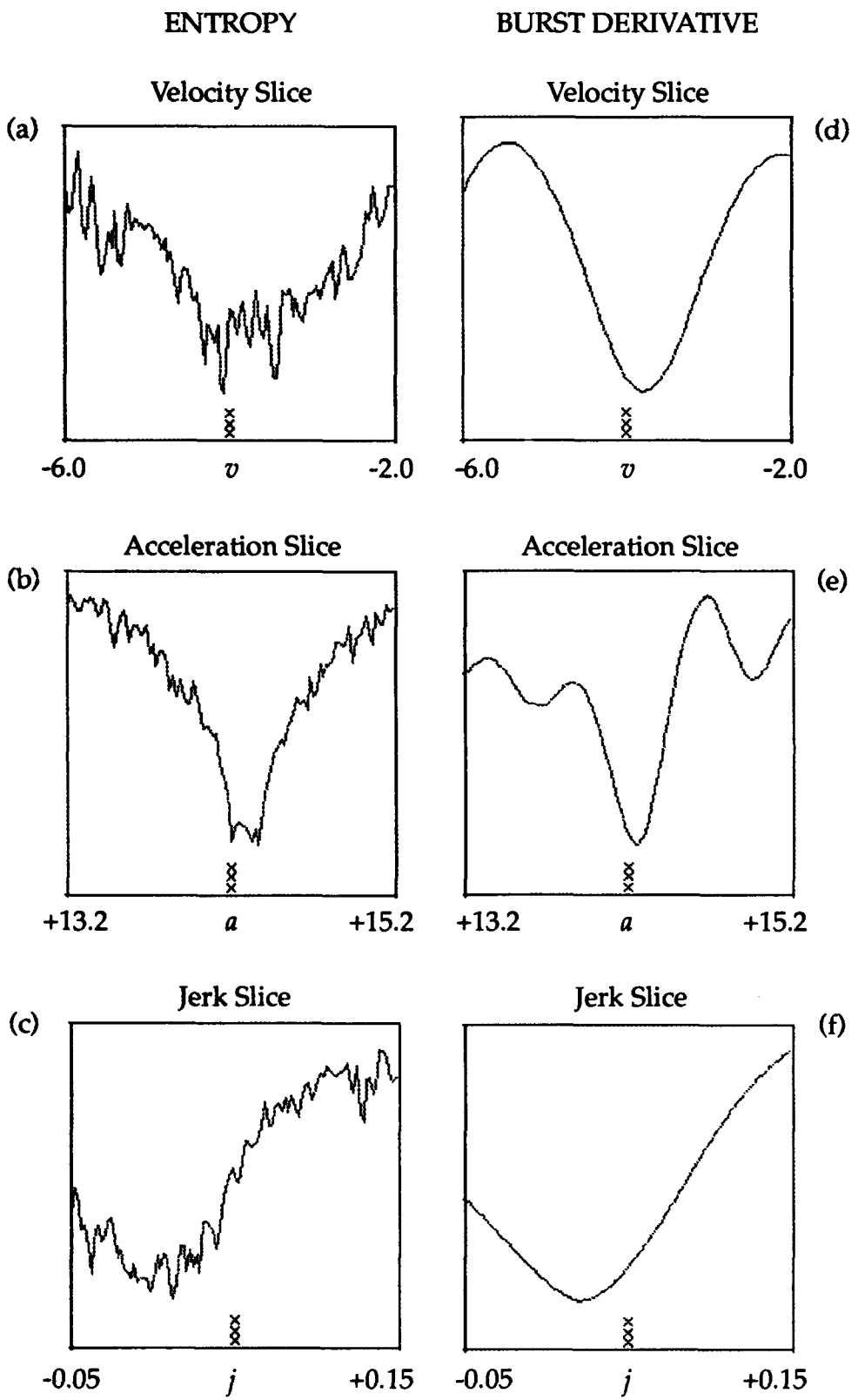

Figure 5. Translational velocity, acceleration, and jerk surface slices.

Figure 6 shows the resulting translational motion-compensated ISAR images obtained using both the entropy and burst derivative measure kinematic estimates in the spatial frequency filter function described by equation 19. Figure 6a shows once again the aircraft reflectivity density function used in this simulation. Figure 6b corresponds to figure 4f and again represents the ideal translational motion-compensated ISAR image obtained using the ground truth values in the spatial frequency filter. Figures 4c and 4d represent the translational motion-compensated ISAR images obtained using the entropy and burst derivative measure kinematic estimates, respectively, in the spatial frequency filter. Listed below each subplot in figure 6 are the corresponding entropy values for that subplot. We see that the ISAR images obtained using the entropy measure and the burst derivative measure are comparable in quality and sharpness to the one obtained using the ground truth information.

In an actual ISAR imaging application, many contiguous (perhaps overlapping) frames of data of a moving aircraft must be processed. From practical experience we have found that the entropy measure must be employed in the TMC algorithm to initially process the first frame of data. This is due to the fact that the entropy surface has a unique global minimum. The burst derivative surface, on the other hand, is periodic with velocity and, therefore, does not have a unique global minimum. However, once the translational kinematics quantities for the first frame have been estimated using the entropy measure, then the burst derivative measure can be used subsequently in the TMC algorithm to track these kinematic quantities and update them as we process additional frames of data in the sequence.

The TMC algorithm has been programmed on a parallel transputer array processor as well. One very important result of that work is that for 64- by 64-pixel array sizes we have found that the burst derivative measure yields translational motion-compensated images of comparable image quality to those obtained using the entropy measure, but does so in approximately one-sixth the time.

Reflectivity Function

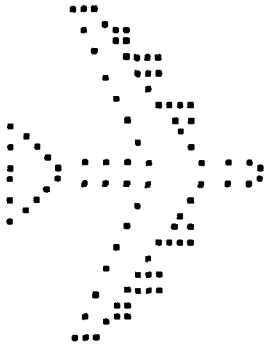

(a)

Ideal Ground Truth Image

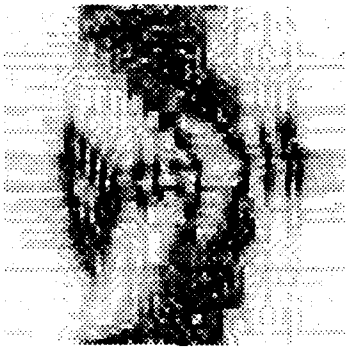

(b) 301

Entropy Processed Image

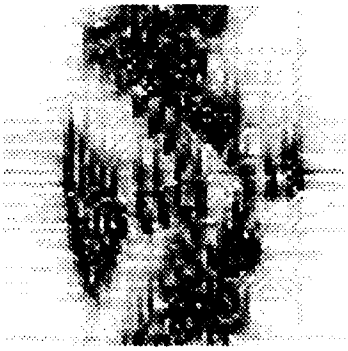

(c) 317

Burst Derivative Processed Image

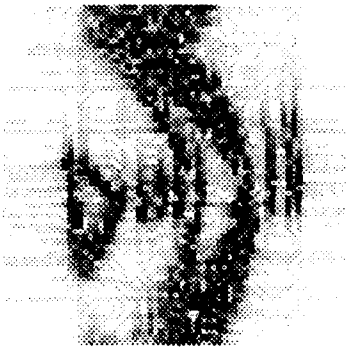

(d) 312

Figure 6. Comparison of translational motion-compensated ISAR images.

6.0 ROTATIONAL MOTION COMPENSATION (RMC) ALGORITHM

Presented in this section is a description of the rotational motion compensation (RMC) algorithm. The objective of the RMC algorithm is to compute an estimate, $\hat{i}(x, y)$, of the ideal final focused ISAR image, *i(x,y)*, by using the output from the TMC algorithm, namely the estimated translational motion-compensated ISAR spatial frequency spectrum $\hat{H}(m, n)$. To do so requires estimating the rotational kinematic quantities ω_o and α_o. Please review figure 3 once again.

The RMC algorithm employs the method of polar reformatting to achieve this objective. In addition, the RMC algorithm in its present form relies heavily on the use of numerous 2D-FFTs needed in the entropy measure calculation for determining the image sharpness. Preliminary results of this investigation indicate that the burst derivative measure employed in the TMC algorithm may be used in lieu of the entropy measure in the RMC algorithm as well. This would have the advantage of eliminating the numerous 2D-FFTs presently required in the entropy measure calculations.

To understand the essential workings of the RMC algorithm, we must first briefly discuss the essential features of polar reformatting. The concept of polar reformatting is described in detail by both Ausherman et al. (1984) and Wehner (1987). Let's initially describe the situation for the case when the ideal translational motion-compensated ISAR spatial frequency spectrum, $H(m, n)$, is known.

Recall that the 2D-FFT of *H(m,n)* led to the ideal translational motion-compensated ISAR image, *h(x,y)*, shown in figure 4f. By polar reformatting the spectral values *H(m,n)*, the ideal final focused ISAR image, *i(x,y)*, shown in figure 4g was obtained. Let's now describe the necessary steps leading to the polar-reformatted image shown in figure 4g.

For the two-dimensional scenario being discussed, the spectral values $H(m, n)$ are physically located on a two-dimensional spatial frequency plane. The Cartesian coordinates describing the position of each value of $H(m, n)$ are specified by the ordered pair of numbers (p_{mn}, q_{mn}) as determined by equation 15. These spectral value coordinates in turn depend on both f_m and θ_{mn} as indicated in equations 16 and 12b, respectively. The angles θ_{mn} depend on the ground truth rotational kinematic quantities θ_o, ω_o, and α_o. Using the ground truth rotational kinematic values and radar parameters listed on page 13 leads to the two-dimensional spatial frequency

domain plots shown in figure 7. Figure 7a depicts a Cartesian set of axes labelled p and q. Each value of (p_{mn}, q_{mn}) obtained from equation 15 is plotted as a point (black dot) in this plane. The wedge-shaped grid pattern resulting in figure 7a represents the region where the 64- by-64 array of ideal spectral values are physical located for the simulation considered in this technical report. A magnified view of this wedge-shaped grid pattern is shown in figure 7b, where the individual black dots comprising the array are now easily distinguishable. In using the 2D-FFT to construct the translational motion-compensated image in figure 4f from *H(m,n)*, it was tacitly assumed that the spectral values *H(m,n)* were located on a rectangular grid pattern, and not on a wedge-shaped grid pattern as seen in figure 7.

Polar reformatting is a technique used to construct a new array of spectral values positioned on a rectangular grid pattern from an array of spectral values lying on a wedge-shaped grid pattern. This new array of spectral values when Fourier transformed will, in general, yield a sharper (more highly focused) ISAR image in comparison to the one obtained when polar reformatting is not used. The polar reformatting technique used for the simulations performed in the Processing Research and Development Branch (Code 761) of the NCCOSC RDT&E Division involves a five-step approach:

1. Oversample the 64-by-64 array of spectral values by a factor of four. This yields a new 256-by-256 array of spectral values.

2. Rotate the newly formed wedge-shaped pattern of 256 by 256 points obtained in step 1 until the wedge bisector lies along the positive p-axis; see figure 8a.

3. Overlay a 64-by-64 rectangular grid pattern of points of maximum extent, but wholly contained within the newly formed wedge-shaped grid pattern obtained in step 2; see figure 8b.

4. At each point on the rectangular grid pattern generated in step 3, find the three nearest neighboring points on the wedge-shaped grid pattern.

5. At each point in the rectangular array, determine a new spectral value by interpolating the spectral values associated with the three nearest neighbor points found in step 4.

Applying this five-step process gives rise to a 64-by-64 rectangular array of spectral values whose discrete Fourier transform yields the desired focused ISAR image, *i(x, y)*, shown in figure 4g.

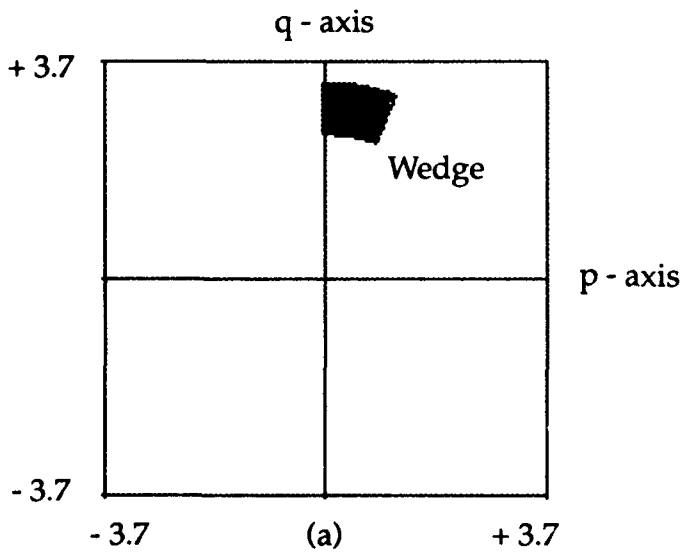

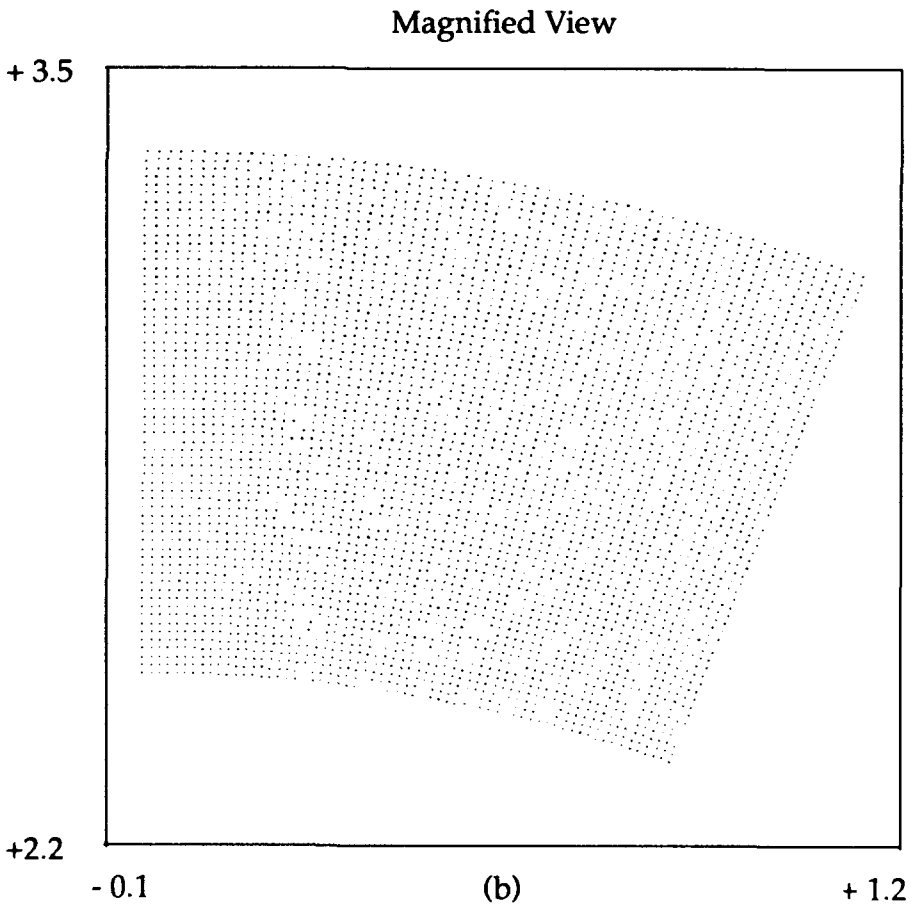

Figure 7. Position of the ideal spatial frequency spectral values.

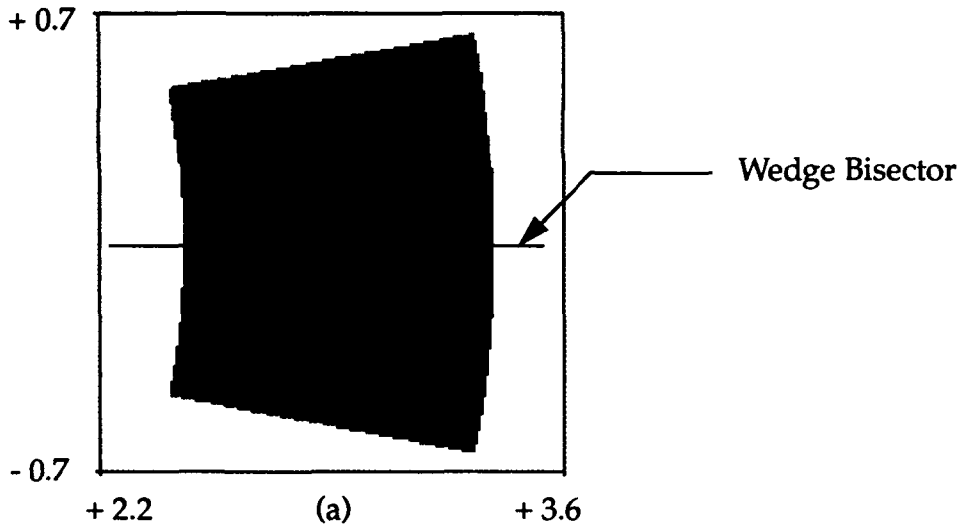

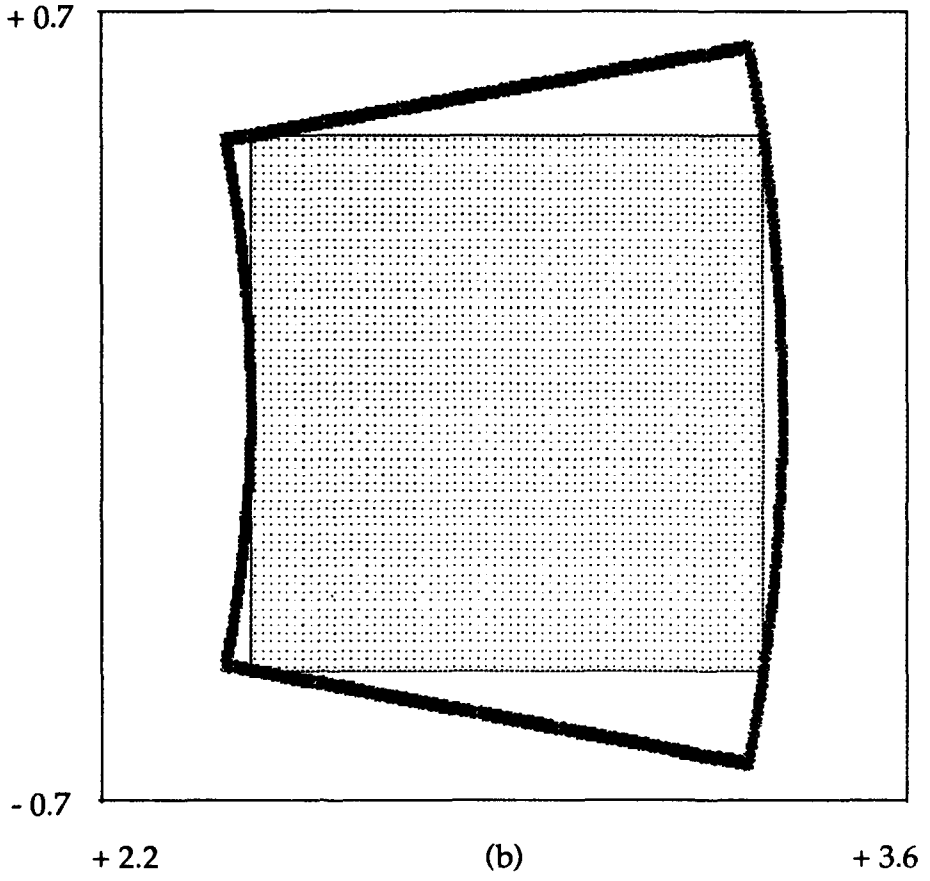

Figure 8. Polar reformatting and interpolation.

The ideal translational motion-compensated spectral values, $H(m,n)$, are, of course, unknown. Hence, the estimated spectral values, $\hat{H}(m,n)$, obtained from the TMC algorithm must be used instead. In addition, the ground truth rotational kinematic quantities of the moving aircraft are also unknown and must be estimated. The following procedure summarizes the key steps of the RMC algorithm.

1. Guess initial values, $\hat{\omega}$ and $\hat{\alpha}$, of the ground truth angular velocity, ω_o, and the angular acceleration, α_o, respectively. Let the estimate, $\hat{\theta}$, of the ground truth rotation angle, θ_o, be zero.

2. Use the values from step 1 with the known values of t_{mn} to generate the quantities θ_{mn} using equation 12b.

3. Use the values from step 2 and the quantities, f_m, from equation 16 to generate the ordered pairs (p_{mn}, q_{mn}) using equation 15.

4. Using the order pairs from step 3, form a wedge-shaped grid pattern analogous to the one formed in figure 7 using actual ground truth data.

5. Apply the five-step reformatting process described on the preceding page to the wedge-shaped grid pattern obtained in step 4 above. This gives an estimated rotational motion-compensated ISAR spatial frequency spectrum, denoted by $\hat{I}(m,n;\hat{\omega},\hat{\alpha})$.

6. Perform a 2D-FFT on the result obtained in step 5. This gives an estimated rotational motion-compensated ISAR image, denoted by $\hat{i}(x,y;\hat{\omega},\hat{\alpha})$.

7. Calculate the entropy of the image obtained from step 6 using the following equation:

$$E(\hat{\omega},\hat{\alpha}) = \sum_{x=0}^{M-1}\sum_{y=0}^{N-1} \left|\hat{i}(x,y;\hat{\omega},\hat{\alpha})\right| \; log\left|\hat{i}(x,y;\hat{\omega},\hat{\alpha})\right|. \tag{25}$$

At this point, new estimates of the rotational kinematic quantities are chosen in step 1, and the above procedure is repeated. This process is repeated over and over again, using a search algorithm similar to the one used in the TMC algorithm, until a minimum value for the entropy is obtained. The estimated rotational kinematic quantities, ω_e and α_e, giving the minimum value of entropy are used as the best estimates of the ground truth

angular velocity and acceleration. The above procedure is applied one last time using the rotational kinematic estimates, ω_e and α_e, to obtain the best estimate, $\hat{i}(x, y)$, of the ideal final focused ISAR image $i(x,y)$, where by definition

$$\hat{i}(x, y) \equiv \hat{i}(x, y; \omega_e, \alpha_e). \tag{26}$$

Also,

$$\hat{I}(m, n) \equiv \hat{I}(m, n; \omega_e, \alpha_e). \tag{27}$$

By using the burst derivative measure (see equation 28 below), we can replace steps 6 and 7 in the RMC algorithm by calculating the burst derivative measure of the polar-reformatted spectrum obtained in step 5 and thus eliminate the multitude of 2D-FFTs presently used when the entropy measure is used in measuring image sharpness.

$$B(\hat{\omega}, \hat{\alpha}) = \sum_{m=0}^{M-1} \sum_{n=0}^{N-1} \left| \frac{\partial}{\partial n} \hat{I}(m, n; \hat{\omega}, \hat{\alpha}) \right|. \tag{28}$$

As in the case of entropy, the burst derivative measure has been employed successfully with an iterative search algorithm to find estimates of ω_e and α_e. Once these estimates are obtained, then only one 2D-FFT is required to form the rotational motion-compensated ISAR image $\hat{i}(x, y)$ from its estimated rotational motion-compensated spectrum $\hat{I}(m, n)$.

7.0 RMC ALGORITHM SIMULATION RESULTS

Preliminary comparisons between the burst derivative measure and the entropy measure in estimating the rotational kinematic quantities of an airborne target have been made. These comparisons have been done with simulated as well as actual ISAR data using a Sun 4 SPARCstation 2. Results typifying the comparison for simulated data on the Sun 4 SPARCstation 2 are presented in this section. In particular, the translational and rotational kinematic quantities (ground truth) as well as radar parameters used in the simulation described on page 13 in section 5 apply here as well. For convenience,

these values are listed below:

$$r_o = 4400\ m \qquad v_o = -4.02\ m/s \qquad a_o = +14.20\ m/s^2 \qquad j_o = +0.05\ m/s^3$$

$$\theta_o = 90.91\ deg \qquad \omega_o = -3.25\ deg/s \qquad \alpha_o = -0.01\ deg/s^2$$

$$M = 64 \qquad N = 64 \qquad \Delta t = 1.59\ ms \qquad f_o = 0.372\ GHz \qquad \Delta f = 2.130\ MHz.$$

First consider the use of the entropy measure in the RMC algorithm for estimating the rotational kinematic quantities of the aircraft. Figure 9 shows angular velocity and angular acceleration slices through the entropy surface described by the entropy function $E(\omega, \alpha)$ defined in equation 25. In particular, figure 9a represents $E(\omega, 0)$ plotted against ω, and figure 9b represents $E(\omega_e, \alpha, 0)$ plotted against α. The quantities ω_e and α_e represent the estimates of the angular velocity and acceleration using the entropy measure. These estimates correspond to the minima of figures 9a and 9b, respectively. The triple x symbol in these subplots represents the position of the ground truth values. Those values of angular velocity and acceleration that gave rise to the minimum value of entropy were $\omega_e = -3.20\ deg/s$ and $\alpha_e = 0.00\ deg/s^2$.

Now consider the use of the burst derivative measure in the RMC algorithm for estimating the rotational kinematic quantities of the aircraft. Figure 9 also shows angular velocity and acceleration slices through the burst derivative surface described by the burst derivative function $B(\omega, \alpha)$ defined in equation 28. Figure 9c represents $B(\omega, 0)$ plotted against ω, and figure 9d represents $B(\omega_e, \alpha)$ plotted against α. The quantities ω_e and α_e in this case represent the estimates of the angular velocity and acceleration using the burst derivative measure. These estimates correspond to the minima of figures 9c and 9d, respectively. Again, the triple x symbol represents the position of the ground truth values. Those values of angular velocity and acceleration that gave rise to the minimum value of burst derivative were $\omega_e = -2.30\ deg/s$ and $\alpha_e = -0.01\ deg/s^2$.

Figure 10 shows the resulting rotational motion-compensated ISAR images obtained using the entropy and burst derivative measure kinematic estimates. Figure 10a shows once again the aircraft reflectivity density function used in this simulation. Figure 10b corresponds to figure 4g and again represents the ideal rotational motion-compensated ISAR image obtained using the ground truth values. Figures 10c and 10d represent the rotational motion-compensated ISAR images obtained using the entropy and burst

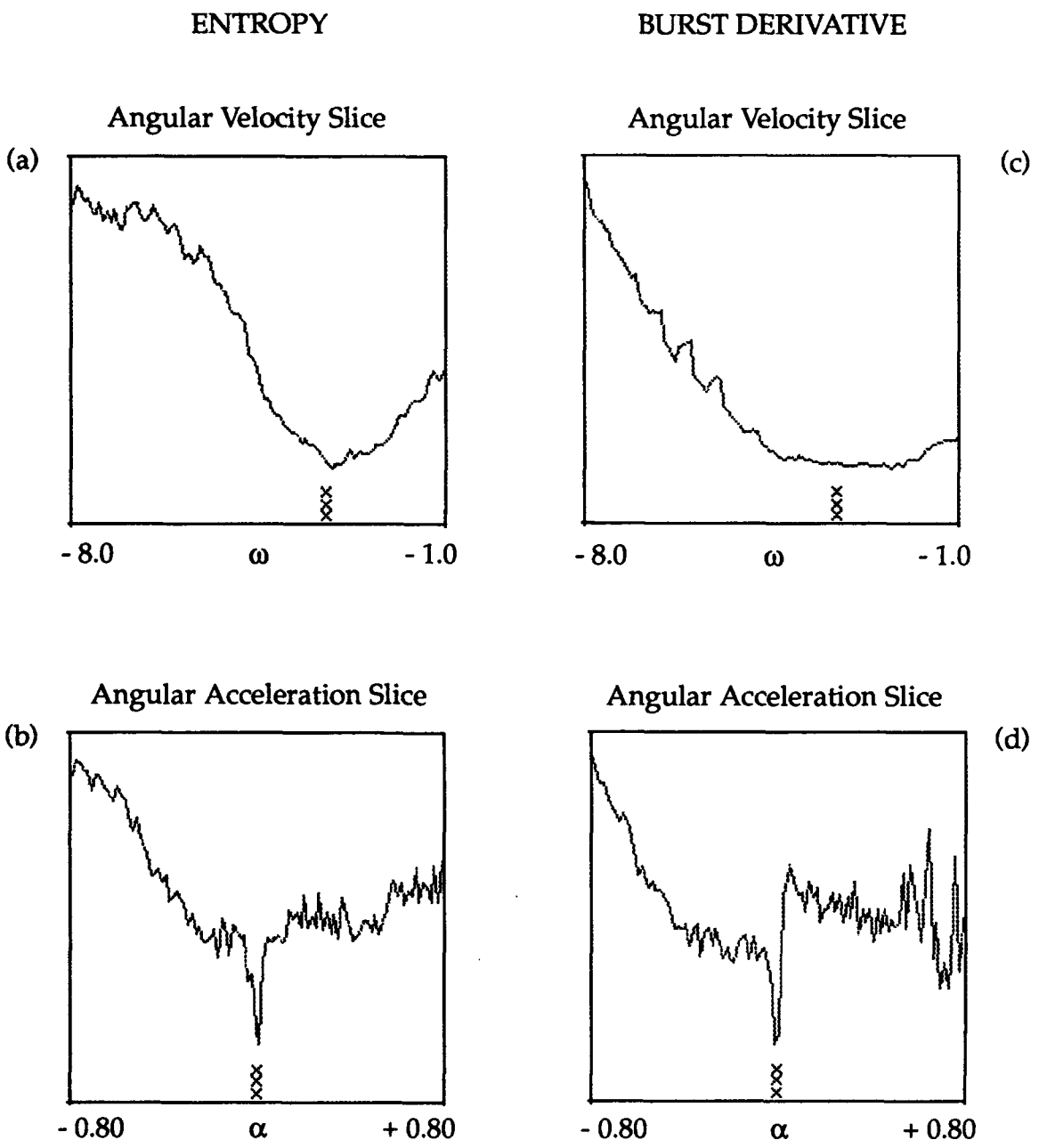

Figure 9. Angular velocity and acceleration surface slices.

Reflectivity Function

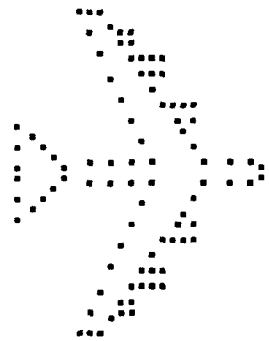

(a)

Ideal Ground Image

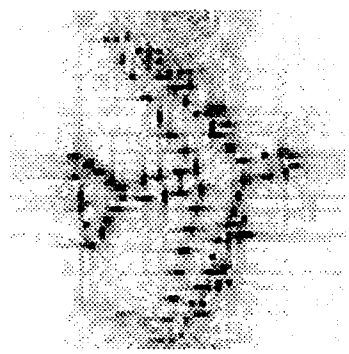

(b) 224

Entropy Processed Image

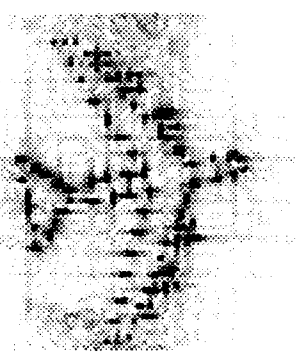

(c) 221

Burst Derivative Processed Image

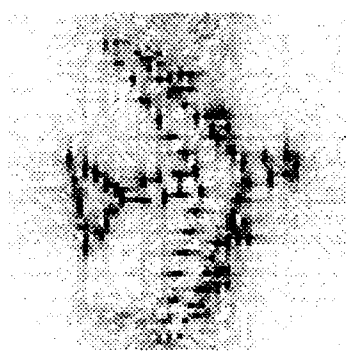

(d) 239

Figure 10. Comparison of rotational motion-compensated ISAR images.

derivative measure kinematic estimates, respectively. Listed below each subplot in figure 10 are the corresponding entropy values for that subplot. We see, once again, that the ISAR images obtained using the burst derivative measure and the entropy measure are comparable in quality and sharpness to the one obtained using the ground truth information.

8.0 TMC AND RMC RESULTS FOR A REAL AIRCRAFT

The results presented in sections 5.0 and 7.0, involving the TMC and RMC algorithms, respectively, are typical of simulations performed to date on a Sun 4 SPARCstation 2 in the Processing Research and Development Branch (Code 761) to test the validity of the burst derivative measure in its ability to predict both the translational and rotational kinematics of an uncooperative airborne target. In this section, we will present results on the use of the TMC and RMC algorithms, using the burst derivative measure, for processing actual ISAR data of a DC-9 commercial airline flying out of Lindbergh Field in San Diego, California. The ISAR data was furnished by the Radar Branch (Code 755) of the NCCOSC RDT&E Division. The pertinent radar parameters used in collecting the ISAR data are

$$M = 64 \qquad N = 64 \qquad \Delta t = 0.146\ ms \qquad f_0 = 9.00\ GHz \qquad \Delta f = 4.00\ MHz.$$

Figure 11 summarizes the results for one frame of ISAR data processed on a Sun 4 SPARCstation 2. Figure 11a represents an array dots depicting the outline of a DC-9 aircraft. This subplot has nothing to do with the actual ISAR data processed. This figure is merely included to remind the reader of the general shape of a DC-9 commercial airliner. Figure 11b is a gray-scale plot of the actual DC-9 unprocessed ISAR spatial frequency spectrum (modulus only plotted). The actual spectral values supplied consisted of a 64-by-64 array of complex numbers. Figure 11c is the gray-scale plot of the unprocessed ISAR image one obtains by taking the 2D-FFT of the unprocessed ISAR spatial frequency spectrum. When the unprocessed ISAR spatial frequency spectrum is multiplied by the spatial frequency filter given by equation 19 for $\hat{v} = v_e, \hat{a} = 0, \hat{j} = 0$, the ISAR image that one obtains by taking the 2D-FFT of the resulting filtered spectrum is shown in figure 11d. Likewise, when the unprocessed ISAR spectrum is multiplied by the spatial frequency filter for $\hat{v} = v_e, \hat{a} = a_e, \hat{j} = 0$, the ISAR image that one obtains from taking the 2D-FFT of the resulting filtered spectrum is shown in figure 11e. Next the unprocessed ISAR spectrum is multiplied by the spatial frequency filter for

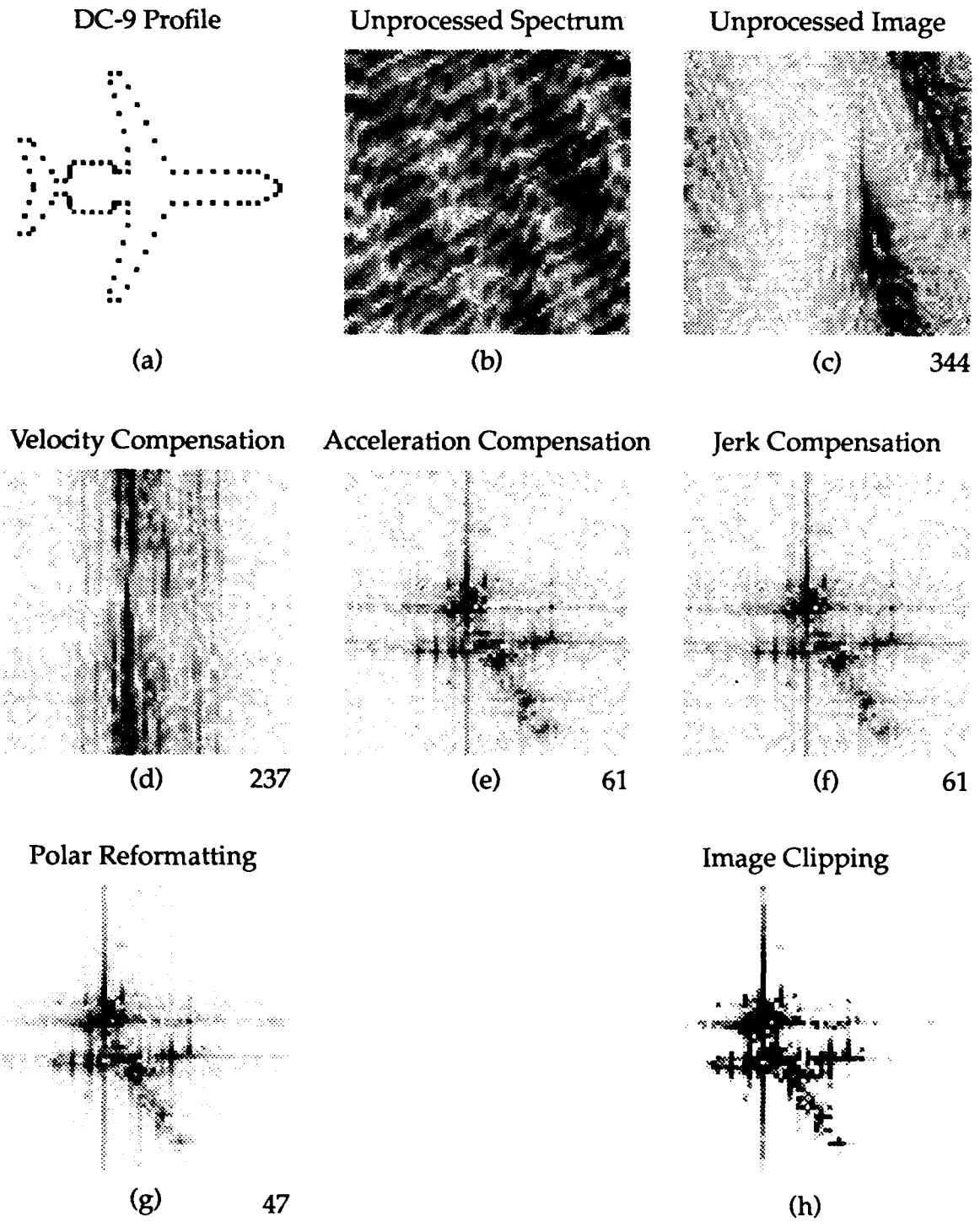

Figure 11. Motion compensation of actual DC-9 ISAR data.

$\hat{v} = v_e, \hat{a} = a_e, \hat{j} = j_e$. The translational motion-compensated ISAR image one obtains by taking the 2D-FFT of the resulting filtered spectrum is shown in figure 11f. Those values of estimated translational velocity, acceleration, and jerk that gave rise to the minimum value of burst derivative measure are given by

$$v_e = -21.3 \ m/s \qquad a_e = -2.4 \ m/s^2 \qquad j_e = 0.00 \ m/s^3.$$

Figure 11g shows the final rotational motion-compensated ISAR image obtained using the burst derivative measure kinematic estimates. Those values of the estimated angular velocity and angular acceleration that gave rise to the minimum value of the burst derivative measure are given by

$$\omega_e = -3.10 \ deg/s \qquad \alpha_e = 0.00 \ deg/s^2.$$

To enhance the contrast of figure 11g, a simple image clipping operation was performed. The result is shown in figure 11h. Pixel values in figure 11g range from 0 to 255 (8-bit quantization). Those values below 175 and above 215 were set to zero. After performing this clipping operation, the remaining non-zero pixel values were normalized, i.e., minimum set to 0 and the maximum to 255. Listed below each subplot in figure 11 are the corresponding entropy values for that subplot.

9.0 CONCLUSIONS

Inverse synthetic aperture radar (ISAR) is an imaging technique that shows great promise in classifying airborne targets in realtime under all weather conditions. The success of classifying targets using ISAR is predicated upon forming highly focused radar images of these targets. Over the past several years, a large body of ISAR data has been collected and considerable effort has been expended to develop algorithms to form high-resolution focused images from these data. Two key algorithms required in processing of ISAR data are the translational motion compensation (TMC) and rotational motion compensation (RMC) algorithms. Vital to each of these algorithms is the ability to measure the sharpness of an image during the iterative computational procedure required to process and focus these images. At the present time, the key figure of merit used to measure image sharpness is entropy. However, a new figure of merit, called the burst derivative measure, offers a reduction in the computational complexity for the TMC and RMC algorithms.

Based on our preliminary investigation of the burst derivative measure, we have reached the following conclusions:

1. **The burst derivative measure is comparable to the entropy measure in terms of its ability to yield highly focused ISAR images.**

   ISAR images have been processed on both a Sun 4 SPARCstation 2 as well as a parallel processing transputer array. The quality and sharpness of images obtained using the burst derivative measure are comparable to those obtained using the entropy measure.

2. **The burst derivative measure offers a speed advantage over the entropy measure.**

   The entropy measure determines image sharpness in real space, whereas the burst derivative measure determines image sharpness in reciprocal space. The spatial frequency filtering operations performed by the TMC algorithm and the polar reformatting and interpolation computations performed by the RMC algorithm are carried out in reciprocal space. Hence, the numerous 2D-FFTs presently required to go from reciprocal space to real space when using the entropy measure can be avoided.

   When tested on a parallel processing transputer array, it was found that the TMC algorithm using the burst derivative measure had a six times speed advantage over the TMC algorithm using the entropy measure for 64-by-64 array sizes.

3. **Entropy must be used in processing the first frame of ISAR data.**

   Entropy is needed to initially estimate the kinematics of the airborne target. Once these estimates have been made, then the burst derivative measure can track the kinematics as they dynamically change in time.

REFERENCES

Ausherman, D. A., A. Kozma, J. L. Walker, H. M. Jones and E. C. Poggio. 1984. "Developments in Radar Imaging," *IEEE Transactions on Aerospace and Electronic Systems*, vol. AES-20, no. 4.

Frieden, B. R. 1989. "Fisher Information as the Basis for Diffraction Optics," *Optics Letters*, vol. 14.

Frieden, B. R. 1990. "Fisher Information, Disorder, and the Equilibrium Distributions of Physics," *Physical Review A*, vol. 41.

Gonzalez, R. C. and P. Wintz. 1987. *Digital Image Processing*, Addison-Wesley, Reading.

Goodman, J. W. 1968. *Introduction to Fourier Optics*, McGraw-Hill, San Francisco.

Wehner, D. R. 1987. *High Resolution Radar*, Artech House, Norwood.

REPORT DOCUMENTATION PAGE

Form Approved
OMB No. 0704-0188

1. AGENCY USE ONLY *(Leave blank)*	2. REPORT DATE	3. REPORT TYPE AND DATES COVERED
	April 1992	Final

4. TITLE AND SUBTITLE
USING THE BURST DERIVATIVE MEASURE TO IMPROVE THE COMPUTATIONAL EFFICIENCY OF ISAR MOTION COMPENSATION ALGORITHMS

5. FUNDING NUMBERS
PE: 0601153N, DB0F
WU: DN301026
DN308026

6. AUTHOR(S)
R. P. Bocker and S. A. Jones

7. PERFORMING ORGANIZATION NAME(S) AND ADDRESS(ES)
Naval Command, Control and Ocean Surveillance Center (NCCOSC)
RDT&E Division (NRaD)
San Diego, CA 92152–5000

8. PERFORMING ORGANIZATION REPORT NUMBER
NRaD TD 2278

9. SPONSORING/MONITORING AGENCY NAME(S) AND ADDRESS(ES)
Office of Naval Research
Arlington, VA 22217

10. SPONSORING/MONITORING AGENCY REPORT NUMBER

11. SUPPLEMENTARY NOTES

12a. DISTRIBUTION/AVAILABILITY STATEMENT
Approved for public release; distribution is unlimited.

12b. DISTRIBUTION CODE

13. ABSTRACT *(Maximum 200 words)*

This technical report describes the use of the burst derivative measure in motion compensation ISAR algorithms for estimating both the slant-range translational motion and rotational kinematic quantities of an uncooperative airborne target. Tests have been performed on simulated as well as actual ISAR data using both a Sun 4 SPARCstation 2 and a parallel processing transputer array. Preliminary results indicate that the burst derivative measure gives significant improvement in processing speed over the traditional entropy measure presently employed.

14. SUBJECT TERMS
burst derivative measure
inverse synthetic aperture radar (ISAR)
ISAR motion compensation algorithms

15. NUMBER OF PAGES
41

16. PRICE CODE

17. SECURITY CLASSIFICATION OF REPORT	18. SECURITY CLASSIFICATION OF THIS PAGE	19. SECURITY CLASSIFICATION OF ABSTRACT	20. LIMITATION OF ABSTRACT
UNCLASSIFIED	UNCLASSIFIED	UNCLASSIFIED	SAME AS REPORT

21a. NAME OF RESPONSIBLE INDIVIDUAL	21b. TELEPHONE *(Include Area Code)*	21c. OFFICE SYMBOL
R. P. Bocker	(619) 553–6404	Code 761

INITIAL DISTRIBUTION

Code 0012	Patent Counsel	(1)
Code 0141	A. Gordon	(1)
Code 575	H. Van Brundt	(1)
Code 70	E. Shutters	(1)
Code 743	H. J. Whitehouse	(1)
Code 7502	B. R. Hunt	(1)
Code 754	D. K. Forbes	(1)
Code 755	R. Dinger	(1)
Code 755	S. Jones	(10)
Code 76	J. R. Wangler	(1)
Code 7601	K. Bromley	(1)
Code 761	G. W. Byram	(1)
Code 761	R. P. Bocker	(70)
Code 80	K. D. Regan	(1)
Code 804	G. W. Beaghler	(1)
Code 804	S. Hoff	(1)
Code 804	E. Munn	(1)
Code 804	J. Zeidler	(1)
Code 843	M. H. Berry	(1)
Code 843	M. Lasher	(1)
Code 844	B. James	(1)
Code 952B	J. Puleo	(1)
Code 961	Archive/Stock	(6)
Code 964B	Library	(2)

Defense Technical Information Center
Alexandria, VA 22304-6145 (4)

NCCOSC Washington Liaison Office
Washington, DC 20363-5100

Center for Naval Analyses
Alexandria, VA 22302-0268

Navy Acquisition, Research & Development
Information Center (NARDIC)
Alexandria, VA 22333

Navy Acquisition, Research & Development
Information Center (NARDIC)
Pasadena, CA 91106-3955